A change in the relation between the Subtropical Indian Ocean Dipole and the

South Atlantic Ocean Dipole indices in the past four decades

Lejiang Yu[1*], Shiyuan Zhong[2], Timo Vihma[3], Cuijuan Sui[4], and Bo Sun[1]

1 MNR Key Laboratory for Polar Science, Polar Research Institute of China,

Shanghai, China,

2 Department of Geography, Environment and Spatial Sciences, Michigan State

University, East Lansing, MI, USA,

3 Finnish Meteorological Institute, Helsinki, Finland

4 National Marine Environmental Forecasting Center, Beijing, China

*Corresponding Author's address Dr. Lejiang Yu

MNR Key Laboratory for Polar Science, Polar Research Institute of China, Shanghai,

China

Jinqiao Road 451, 200136, Shanghai, China

Phone: 0086-020-58712034, email: yulejiang@sina.com.cn

Abstract

   We utilized the global atmospheric reanalysis (ERA5) and reconstructed sea

surface temperature (SST) data from 1979 through 2020 to examine the stability of

the relationship between the SST oscillations in the southern Indian and the Atlantic

Oceans described by the Subtropical Indian Ocean Dipole (SIOD) and the South

Atlantic Ocean Dipole (SAOD) indices. We note a significant positive correlation

between the two indices prior to the year 2000 but practically no correlation

afterwards. We show that in the two decades prior to 2000, a positive phase of SAOD

is associated with more convective activities over the subtropical southern Atlantic

Ocean and eastern Brazil, which trigger a stronger upper-atmosphere wavetrain, and

further produces stronger southern subtropical highs and surface anti-cyclonic

circulations and therefore a stronger correlation between the two indices. The

situation is reversed after 2000. Our results are potentially applicable for predictions

of precipitation in southern Africa and South America.

1   Introduction

   A southwest-northeast-oriented dipole mode characterizes the anomalous sea

surface temperature (SST) patterns over the subtropical South Indian and Atlantic

Oceans (Wang, 2010). The former is referred to as the Subtropical Indian Ocean

Dipole (SIOD) mode (Behera and Yamagata, 2001) and the latter is named as the

South Atlantic Ocean Dipole (SAOD) mode (Venegas et al., 1997). The two

subtropical modes display similar seasonal variability with their peaks in austral

summer (Morioka et al., 2012). Surface latent heat flux anomalies play a vital role in

45   their variability (Sterl and Hazeleger, 2003; Suzukietal., 2004; Hermes and Reason,

46   2005). Moreover, the interannual variability of the two modes has been linked to the

47   El Niño–Southern Oscillation (ENSO) (Boschat et al., 2013). The two subtropical

48   modes exert a great influence on precipitation in Africa and South America (Reason,

49   2001; 2002; Vigaud et al., 2009; Nnamchi and Li, 2011; Morioka et al., 2012; Wainer

50   et al., 2020) and, therefore, understanding the relationship between the two modes has

51   practical implications for precipitation forecasts in Africa and South America on

52   seasonal scale and beyond.

53   Using observational data, Fauchereau et al. (2003) noted the co-variability of the

54   SIOD and SAOD indices in austral summer. Hermes and Reason (2005) confirmed

55   the co-variability of the two indices and attributed it to an anomalous subtropical high.

56   Both studies suggested a linkage between the two indices and an atmospheric zonal

57   wavenumber-4 pattern in the Southern Hemisphere. Lin (2019) also suggested the

58   atmospheric zonal wavenumber-4 pattern controlling the South Atlantic-South Indian

59   Ocean SST pattern. The atmospheric wavenumber-4 was also observed in other

60   studies (Chiswell, 2021; Senapati, et al., 2021). The global wavenumber-4 pattern in

61   SST includes southern subtropical Indian and Atlantic Ocean components that

62   resemble the two subtropical dipole modes (Senapati et al., 2021). The linkage

63   between the SST patterns in the Southern Hemisphere ocean basins and their relation

64   with atmospheric wavenumber-4 pattern is a challenging and active research topic

65   worthy of further investigation.

66   Although previous studies have suggested that a relationship exists between the

67 SIOD and the SAOD indices, few have focused on the stability of the relationship. In

68 this study, we examine the SIOD-SAOD relationship over the past four decades from

69 1979 through 2020. We underscore a change in the relationship that occurred around

70 2000 and provide a physical explanation for the change.

2   Datasets and methods

72 Monthly SST data from the United States National Oceanic and Atmospheric

73 Administration (NOAA) Extended Reconstucted SST V5 (Huang et al., 2017) is the

74 primary dataset utilized to calculate the SIOD and SAOD indices. A secondary SST

75 data, the Kaplan Extended SST V2 data set from the UK Met Office (Kaplanet al.,

76 1998), is also used to confirm the results. Following previous studies, we derive the

77 SIOD index as the difference in the SST anomalies between the western (55-65 °E,

78 37-27 °S) and eastern (90-100 °E, 28-18 °S) subtropical Indian Ocean (Behera and

79 Yamagata, 2001) and the SAOD index as the difference of SST anomalies between

80 the south-western (10-30 °W, 30-40 °S) and north-eastern (0-20 °W, 15-25 °S) South

81 Atlantic Ocean (Morioka et al., 2011). Atmospheric data from the European Centre

82 for Medium-Range Weather Forecasts (ECMWF) fifth-generation reanalysis (ERA5,

83 Hersbach et al., 2020) provide the upper-level (200-hPa) and surface atmospheric

84 variables used in our analyses except for the monthly top-of-atmosphere (TOA)

85 outgoing longwave radiation (OLR) that is from the NOAA Interpolated OLR dataset

86 (Liebmann and Smith, 1996). For SST or atmospheric variables, the anomalies refer

87 to the departure from their climatology computed as the 42-year averaged value.

88 Correlation and regression analyses are utilized to examine the relationship

89   between the SIOD and the SAOD indices. The confidence levels are determined by

90   the two-tailed Student's t test. Before the correlation or regression analyses are

91   applied to the data, the variables and indices are detrended. We also remove the

92   influence from the ENSO signal using the method proposed by An (2003), where the

93   ENSO signal is represented by the Niño 3.4 index. The generation and propagation of

94   planetary waves are identified on the basis of the Rossby wave source (RWS) and the

95   wave activity flux (WAF). The RWS is calculated following Sardeshmukh and

96   Hoskins (1988) and the WAF is derived using the method of Takaya and Nakamura

97   (2001). Notice that due to the peak of the SIOD and SAOD in February (Morioka et

98   al., 2012), the austral seasons in this study refer to summer (January-March), autumn

99   (April-June), winter (July-September), and spring (October-December).

100 **3   Results**

101   The regressed SIOD and SAOD indices on detrended SST anomalies display

102   southwest-northeast-oriented dipoles in the subtropical southern Indian Ocean (Figure

103   1a) and Atlantic Ocean (Figure 1b). The correlations between the SIOD and SAOD

104   indices over the 42-year period are 0.56 for austral summer ($p<0.05$), becoming

105   insignificant in other seasons with correlation coefficients dropping by nearly half to

106   0.23 for austral autumn and winter and 0.25 for austral spring. Removing the ENSO

107   signal resulted in small changes in the correlations and their seasonal variations, with

108   summer being the only season when the two indices are significantly correlated (0.45,

109     $p<0.01$) (Figure 1c). The Kaplan Extended SST V2 data yielded similar results, with

110   slightly lower summertime correlation coefficients of 0.49 (with ENSO signal) and

111   0.38 (without ENSO signal, p<0.05). Henceforth, we focus on the summer time series

112   without the ENSO signal.

113   To assess the stability of the SIOD-SAOD correlation over the past four decades,

114   we calculate moving correlation of the two indices using 15-year and 20-year sliding

115   windows (Figure 1d). For the 15-year window, the correlation is above (below) the 95%

116   confidence level before (after) 1998 and for the 20-year sliding window the shifting

117   occurs in 2003. Similar results are obtained using the Kaplan Extended SST V2 data

118   (Figure 2). There is a remarkable difference in the correlation between the two indices

119   prior to and after 1999 (Figure 1d). For the 1979-1999 period, the correlation

120   coefficient is 0.64 (p<0.01), dropping sharply to only 0.19 (p>0.05) for the 2000-2020

121   period. Results derived using the Kaplan Extended SST V2 data are very similar, with

122   the correlation coefficients of 0.60 (p<0.01) for the 1979-1999 period and 0.20

123   (p>0.05) for the 2000-2020 period. This notable drop in the correlation between the

124   SIOD and SAOD indices from the first two decades to the next two warrants further

125   investigation. Below we explore the reasons behind the change.

126   We compare the regression maps of the Southern Hemisphere SST anomalies on

127   the summertime SAOD and SIOD indices for the 1979-1999 period with those for the

128   2000-2020 period (Figure 3). There are clear differences in the anomalous SST

129   patterns between the two periods. As a response to the positive phase of the SAOD

130   index, significant SST anomalies occur in the southern subtropical Indian Ocean

131   during the 1979-1999 period, with a spatial pattern (Figure 3a) closely resembling the

132   positive phase SIOD index (Figure 1a); however, the SST anomalies for the

133   2000-2020 period are not significant in the southern subtropical Indian Ocean (Figure

134   3b). Similarly, corresponding to the SIOD index, a dipole of significant SST

135   anomalies appears in the South Atlantic Ocean (Figure 3c) for the 1979-1999 period

136   that bear strong resemblance to the positive phase SAOD pattern (Figure 1b), whereas

137   for the 2000-2020 period, the SST anomalies are insignificant (Figure 3d). These

138   results confirm the strong correlation between the SAOD and SIOD indices during the

139   first two decades and the lack of correlation in the last two decades, separated by the

140   turn of the century. The SST anomalies in Figure 3 display the appearance of the SST

141   wavenumber-4 mode (Senapati et al., 2021), including the SIOD and SAOD pattern.

142   Senapati et al. (2022) suggested that the weakening of the SST wavenumber-4 pattern

143   after 2000 is related to South Pacific Meridonal Mode. In addition, the weaker

144   SIOD-SAOD relationship after 2000 may be related to the decadal variability of a

145   warm pool dipole, with opposite SST anomalies in the southeastern Indian Ocean and

146   the western-central tropical Pacific Ocean (Zhang et al., 2021).

147   Lin (2019) related a South Atlantic-South Indian Ocean pattern to a wavetrain

148   induced by the South Atlantic Convergence Zone anomaly. We hypothesize that the

149   stability of the SAOD-SIOD relation may also be related to the strength of the

150   wavetrain. To test this hypothesis, we examine the regression patterns of several

151   atmospheric variables related to convective and wave activities (OLR, RWS, WAF,

152   200-hPa divergent wind, and streamfunction) to the SAOD index in austral summer

153   separately for the 1979-1999 period and the 2000-2020 period (Figure 4). Over the

154   1979-1999 period, corresponding to the positive phase of the SAOD index,

155 convective activities are enhanced over the southern subtropical Atlantic Ocean and

156 eastern Brazil, which are flanked by suppressed convective activities over tropical and

157 mid-latitude South Atlantic Ocean (Figure 4a). The convective activities over western

158 subtropical southern Atlantic Ocean and eastern Brazil produce positive RWS and

159 200-hPa divergent wind (Figure 4c),which trigger a wavetrain propagating

160 southeastwards into the South Atlantic Ocean, and then eastwards into the South

161 Indian Ocean, Australia and the South Pacific Ocean (Figure 4e). The wavetrain

162 generates negative streamfunction anomalies over the South Indian and Atlantic

163 Oceans (Figure 4e). In contrast, over the 2000-2020 period, the magnitude of the

164 anomalous OLR is less significant than that over the 1979-1999 period (Figure 4b).

165 Weaker RWS and upper level divergent wind (Figure 4d) indicate a weaker wavetrain,

166 which results in weaker streamfunction anomalies over the South Atlantic and Indian

167 Oceans (Figure 4f). To show clearly the RWS, upper-level divergent wind and Rossby

168 wavetrain, we show the significant areas in Figures 4c-f in supplementary file

169 (Figures S1)

170   Although the magnitudes of the OLR anomalies related to the SAOD index are

171 comparable over the two periods (Figure 4a and 4b), the anomalous OLR and RWS

172 and the related wavetrain associated with the SAOD index are substantially different

173 between the two periods. The differences in the climatological conditions over the two

174 periods may provide a plausible explanation. For example, over the subtropical

175 southern Atlantic Ocean and most of Brazil, the climatological OLR anomalies are

176 generally negative during the 1979-1999 period, suggesting stronger convective

activity favorable for the generation of the wavetrain (Figure 5a), but in contrast, OLR

anomalies are mostly positive during 2000-2020, indicating suppressed convective

activities unfavorable for the formation of the wavetrain (Figure 5b). Thus, the

interdecadal variability of the OLR activities can modulate the effect of the SAOD

mode on atmospheric circulation patterns over other ocean basins.

The SAOD and SIOD modes are related to the subtropical highs in the South

Atlantic and Indian Oceans, with stronger high corresponding to the positive phase of

the two indices due to wind-induced evaporation (Wang, 2010; Behera and Yamagata,

2001; Venegas et al., 1997). We proceed to examine the climatological mean sea level

pressure and surface wind field related to the aforementioned wavetrain over the two

periods (Figure 6). The position and strength of the climatological subtropical highs

and the associated surface winds in the southern Indian and the Atlantic Oceans show

little difference over the two periods (Figure 6a and 6b). However, the regression of

the mean sea level pressure to the SAOD index for the two periods show considerably

stronger subtropical highs and anti-cyclonic circulations in the South Atlantic and the

Indian Oceans over the 1979-1999 period than the 2000-2020 period (Figure 6c and

6d). According to the study of Hermes and Reason (2005), a stronger subtropical high

favors larger magnitude of the SST anomalies represented by the SAOD and SIOD

indices. The large decrease in the strength of the summertime subtropical high

associated with SAOD from the first two decades to the next two (Figure 6c, 6d)

corroborates the sharp drop in the SAOD-SIOD correlation (Figure 1d). Prior to 2000,

the stronger wavetrain associated with SAOD induced stronger summertime

subtropical highs, which produced larger subtropical SST anomalies in both basins, strengthening the SASD-SIOD relationship. After 2000, the weaker wavetrain induced weaker subtropical highs. The SST anomalies in each basin are largely determined by the physical processes in each basin, which is not directly related to the wavetrain. Thus, the SAOD-SIOD relationship is weaker after 2000.

Similarly, we have also obtained the patterns of the aforementioned atmospheric circulation variables associated with the SIOD index separately for the two periods (Figure 7). During 1979-1999, negative OLR anomalies occur over the northern South America, corresponding to upper-level divergent wind and positive RWS anomalies, while positive OLR anomalies exist over the southern Atlantic Ocean, leading to upper-level convergent wind and negative RWS anomalies (Figure 7a and 7c). Those anomalous RWSs produce an anomalous Rossby wavetrain propagating from the southern Atlantic Ocean to southern Indian Ocean (Figure 7e). During 2000-2020, negative (positive) OLR anomalies over the tropical (subtropical) central Pacific Ocean generate anomalous upper-level winds and RWSs, which excite a wavetrain propagating from the Pacific to South America and the southwestern South Atlantic Ocean (Figure 7b, 7d, and 7f). Meanwhile, stronger convective activities over the southwestern Indian Ocean and weaker convective activities over central Indian Ocean also produce anomalous RWSs, which trigger a local wavetrain propagating eastwards into Australia. However, the two wavetrains are controlled by different factors and are not connected to each other over the South Atlantic Ocean. We also examine the MSLP and surface wind field related to the SIOD index in austral

221   summer for the 1979-1999 and 2000-2020 periods (Figure 8). Over the 1979-1999

222   period, stronger subtropical highs develop over the South Indian and Atlantic Oceans,

223   which induce the positive phase of the SIOD and SAOD modes, respectively (Figure

224   8a), suggesting that the SIOD and SAOD index is connected to each other through the

225   aforementioned wavetrain (Figure 7e). Over the 2000-2020 period, positive MSLP

226   anomalies and anomalous anticyclonic circulation dominate over the South Indian

227   Ocean, though negative MSLP anomalies and anomalous cyclonic circulation occur

228   over the southwestern South Indian Ocean (Figure 8b). The atmospheric circulation

229   anomalies over the South Indian Ocean are related to the OLR anomalies and induced

230   a local wavetrain (Figure 7b, 7d and 7f). Similarly, the significant areas in Figures

231   7c-f are shown in supplementary file (Figures S1). The positive MSLP anomalies and

232   anticycloinic circulation anomalies are absent over the South Atlantic Ocean (Figure

233   8b). These results indicate that the SIOD mode over the 2000-2020 period is related to

234   local convective activities, not to those over the South Atlantic Ocean.

235   **4   Conclusion and discussion**

236   In this study, we examined the relation between the oscillations of the SST in the

237   subtropical South Indian and the Atlantic Oceans described by the SIOD and SAOD

238   indices and the stability of the relation using the ERA5 global atmospheric reanalysis

239   and reconstructed SST data from 1979 through 2020. We found significant relation

240   between the two indices in austral summer. Through moving correlation analyses, we

241   discovered that the relation in austral summer was not stable for the past four decades.

242   Specifically, the correlation between the two indices was significant prior to 2000 but

243   insignificant afterwards. The change in the relation between the two indices is

244   attributed to a change in the strength of the atmospheric wavetrain induced by

245   anomalous convective activity over the subtropical southern Atlantic Ocean and

246   eastern Brazil. More frequent and stronger convective activities prior to 2000 excited

247   stronger wavetrain, which produced stronger subtropical highs during the positive

248   phase of SAOD, resulting in a stronger relation between the two indices. The opposite

249   occurred after 2000.

250   The interdecadal variability of OLR over the subtropical South America and

251   Atlantic Ocean is the key to the relation between the SAOD and SIOD indices. What

252   determined the OLR anomalies in the region prior to and after 2000 needs to be

253   further investigated. Hermes and Reason (2005) suggested that the southern

254   subtropical high is related to the Antarctic Oscillation (AAO) and the linkage

255   strengthened after mid-1970s. The influence of the change in the AAO index on the

256   relation between the SAOD and the SIOD indices needs to be assessed. Yu et al.

257   (2017) noted a phase change of the Atlantic Multidecadal Oscillation (AMO) and the

258   Pacific Decadal Oscillation (PDO) indices in the late 1990s, with PDO shifting from

259   positive to negative and AMO switching from negative to positive around 1999. Dong

260   and Dai (2015) noted the influence of IPO on precipitation in Brazil. However, the

261   influence from the same phase of the IPO has great uncertainty and depends on the

262   period and dataset (Dong and Dai, 2015). Jones and Carvalho (2018) suggested more

263   precipitation in Brazil during the negative phase of the AMO than during its positive

264   phase. Longer datasets are utilized to examine the effect of the IPO and AMO on

convective activity over the subtropical South America and Atlantic Oceanon the

interdecadal time scale. Although our results are only based on statistical analyses,

they have potential for improving the prediction of precipitation in southern Africa

and South America.

Data Availability

The monthly SST data from the U.S. NOAA Extended Reconstructed Sea Surface

Temperature (ERSST) version 5 (ERSST v5) are available online

(https://www1.ncdc.noaa.gov/pub/data/cmb/ersst/v5/netcdf/).Kaplan Extended SST

V2 data are derived from below website

(https://psl.noaa.gov/cgi-bin/db_search/DBSearch.pl?Dataset=Kaplan+Extended+SST

+V2&Variable=Sea+Surface+Temperature).The monthly ERA5 reanalysis data are

available from the Copernicus Climate Data Store

(https://www.ecmwf.int/en/forecasts/datasets/reanalysis-datasets/era5). The monthly

OLR data are derived from the NOAA Interpolated OLR

(https://psl.noaa.gov/cgi-bin/db_search/DBSearch.pl?Dataset=NOAA+Interpolated+O

LR&Variable=Outgoing+Longwave+Radiation).

Acknowledgments

We thank the European Centre for Medium-Range Weather Forecasts (ECMWF) for

the ERA5 data. This study is financially supported by the National Key R&D

Program of China (2022YFE0106300), the National Science Foundation of China

(41941009), and the European Commission H2020 project Polar Regions in the Earth

System (PolarRES; Grant101003590).

287 *Author contributions*. LY designed the research, analyzed the data, and wrote the first

288 draft of the paper. S Z and TV revised the first draft and provided useful insights

289 during various stages of the work. CS and BS provided some comments and helped

290 with editing the paper.

291 *Competing interests*. The authors declare that they have no conflict of interest.

292 **References**

293 An, S. I.: Conditional maximum covariance analysis and its application to the

294   tropical Indian Ocean SST and surface wind stress anomalies, J. Climate, 16,

295   2932–2938, 2003.

296 Behera, S. K., and Yamagata, T.: Subtropical SST dipole events in the southern

297   Indian Ocean, Geophys. Res. Lett., 28, 327-331, 2001.

298 Boschat, G, Terray, P., and Masson, S.: Extratropical forcing of ENSO, Geophys. Res.

299   Lett., 40, 1605-1611, 2013.

300 Chiswell, S. M.: Atmospheric wavenumber-4 driven South Pacific marine heat waves

301   and marine cool spells, Nature Communication, 12, 4779, 2021.

302 Dong, B., and Dai, A.: (2015).The influence of the Interdecadal Pacific Oscillation on

303   temperature and precipitation over the global, Clim. Dyn., 45, 2667-2681.

304 Fauchereau, N., Trzaska, S., Richard, Y., Roucou, P., and Camberlin, P.: Sea

305   Surface temperature co-variability in the Southern Atlantic and Indian Oceans

306   And its connections with the atmospheric circulation in the Southern

307   Hemisphere, Int. J. Climatol., 23, 663–677, 2003.

308 Hermes, J. C., and Reason, C. J. C.: Ocean model diagnosis of interannual coevoling

309   SST variability in the South Indian and South Atlantic Oceans, J. Climate, 18,

310   2864-2882, 2005.

311 Hersbach, H., Bell, B., Berrisford, P., Hirahara, S., Horányi, A., Muñoz-Sabater, J.,

312   Nicolas, J., Peubey, C., Radu, R., Schepers, D., Simmons, A., Soci, C., Abdalla,

313   S., Abellan, X., Balsamo, G., Bechtold, P., Biavati, G., Bidlot, J., Bonavita, M.,

314   De Chiara, G., Dahlgren, P., Dee, D., Diamantakis, M., Dragani, R., Flemming,

J., Forbes, R., Fuentes, M., Geer, A., Haimberger, L., Healy, S., Hogan, J. R., Hólm, E., Janisková, M., Keeley, S., Laloyaux, P., Lopez, P., Lupu, C., Radnoti, G., de Rosnay, P. Rozum, I., Vamborg, F., Villaume, S., and Thépaut J.-N.: The ERA5 global reanalysis, Quarterly Journal of the Royal Meteorological Society, 146, 1999-2049, 2020.

Huang, B., Thorne, P. W., Banzon,V. F., and Zhang, H. M.: Extended Reconstructed SeaSurface Temperature version 5 (ERSSTv5), Upgrades, validations, and Intercomparisons, J. Climate, 30, 8179-8205, 2017.

Jones, C., and Carvalho, L. M. V.: The influence of the Atlantic multidecadal oscillation on the eastern Andes low-level jet and precipitation in South America, npj Climate and Atmospheric Science, 1, 40, 2018.

Kaplan, A., Cane, M., Kushnir, Y., Clement, A., Blumenthal, M., and Rajagopalan, B.: Analyses of global sea surface temperature 1856-1991, J. Geophys. Res., 103, 18567-18589, 1998.

Liebmann, B., and Simth, C. A.: Description of a complete (interpolated) outgoinglongwave radiation dataset, Bulletin of the American Meteorological Society, 77, 1275–1277, 1996.

Morioka, Y., Tozuka, T., and Yamagata, T.: On the growth and decay of the subtropical dipole mode in the south Atlantic. J. Climate, 24, 5538-5554, 2011.

Morioka, Y., Tozuka, T., Masson, S., Terray, P., Luo, J.-J., and Yamagata, T.: Subtropical dipole modes simulated in a coupled general circulation mode, J. Climate, 25, 4029-4047, 2012.

Nnamchi, H. C., and Li, J. P.: Influence of the South Atlantic Ocean Dipole on West African summer precipitation, J. Climate, 24, 1184-1197, 2011.

Reason, C. J. C.: Subtropical Indian Ocean SST dipole events and southern African rainfall, Geophys. Res. Lett., 28, 2225–2227, 2001.

Reason, C. J. C.: Sensitivity of the southern African circulation to dipole sea-surface temperature patterns in the South Indian Ocean, Int. J. Climatol., 22, 377–393, 2002.

Sardeshmukh, P. D., and Hoskins, B. J.: The generation of global rotational flow

345   by steady idealized tropical divergence, J. Atmos. Sci., 45, 1228–1251, 1988.

346   Senapati, B., Deb, P., Dash, M. K., and Behera, S. K.: Origin and dynamics of

347   global atmospheric wavenumber-4 in the Southern mid-latitude during austral

348   summer. Climate Dynamics, doi:10.1007/s00382-021-06040-z, 2021.

349   Senapati, B., Dash, M. K., and Behera, S. K.: Global wave number-4 pattern in

350   the southern subtropical sea surface temperature, Scientific Reports, 11, 142,

351   doi:10.1038/s41598-020-80492-x, 2021.

352   Senapati, B., Dash, M. K., and Behera, S. K.: Decadal variability of southern

353   subtropical SST wavenumber-4 pattern and its impact. Geophysical Research

354   Letters, e2022GL099046. doi:10.1029/2022GL099046, 2022.

355   Sterl, A., and Hazeleger, W.: Coupled variability and air-sea interaction in the

356   South Atlantic Ocean. Climate Dyn., 21, 559–571, 2003.

357   Suzuki,R.,Behera,S.K., Iizuka,S., and Yamagata, T.: IndianOcean Subtropical dipoles

358   simulated using a coupled general circulation model. J. Geophys. Res., 109,

359   C09001, doi:10.1029/2003JC001974, 2004.

360   Takaya, K., and Nakamura, H.: A formulation of a phase in dependent wave-activity

361   flux for stationary and migratory quasi geostrophic eddies on a zonally varying

362   basic flow. J. Atmos. Sci., 58, 608–627, 2001.

363   Vigaud, N., Richard, Y., Rouault, M., and Fauchereau, N.: Moisture transport between

364   The South Atlantic Ocean and southern Africa: Relationships with summer

365   rainfall and associated dynamics. Climate Dyn., 32, 113–123, 2009.

366   Venegas, S. A., Mysak, L. A., and Straub, D. N.: Atmosphere–ocean coupled

367   variability in the South Atlantic, J. Climate, 10, 2904–2920, 1997.

368   Wainer, I., Prado, L. F., Khodri, M., and Otto-Bliesner, B.: The South Atlantic

369   subtropical dipole mode since the last deglaciation and changes in rainfall,

370   Climate Dynamics, 56,109-122, doi:10.1007/s00382-020-05468-z, 2020.

371   Wang, F.: Subtropical dipole mode in the Southern Hemisphere: A global view.

372   Geophs. Res. Lett., 37, L10702, doi:10.1029/2010GL042750, 2010.

373 Yu, L., Zhong, S., Winkler, J. A., Zhou, M., Lenschow, D. H., Li, B., Wang, X., and

374   Yang, Q.: Possible connection of the opposite trends in Arctic and Antarctic

375   sea ice cover. Scientific Reports, 7, 45804, 2017.

376 Zhang, L., Han, W., Karnauskas, K. B., Li, Y., and Tozuka, T.: Eastward shift of

377   Interannual climate variability in the South Indian Ocean since 1950.

378   Journal of Climate, 35, 561-575.

379

380

381
382
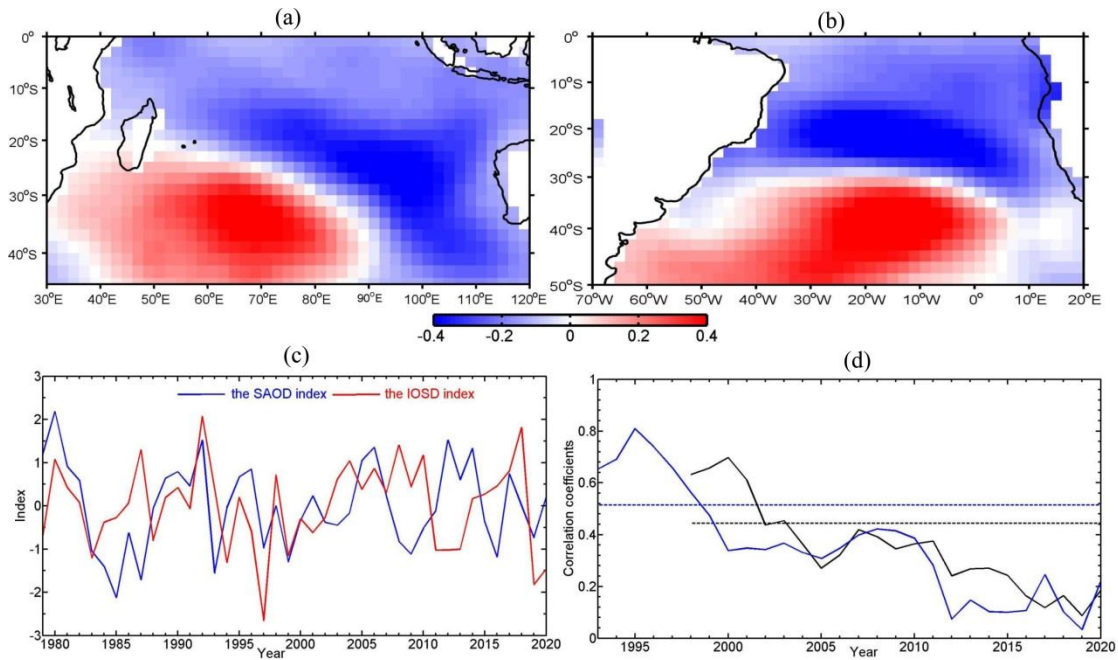
Figure 1. Regression patterns of austral summer (JFM) SST anomalies (°C) on the positive phase of the summertime indices of (a) the Subtropical Indian Ocean Dipole (SIOD), (b) the South Atlantic Ocean Dipole (SAOD), (c) their time coefficients, and (d) the moving correlations between the detrended and ENSO-signal-removed SIOD and SAOD indices (time coefficients) using a 20-year (black solid line) and a 15-year (blue solid line) sliding window. In (d), the dashed lines denote the correlation coefficients with the 95% confidence level for 20 (black) and 15 (blue) samples and the abscissa indicates the end year of the moving correlations. The above results are derived using the NOAA Extended Reconstucted SST V5 data.

391

392
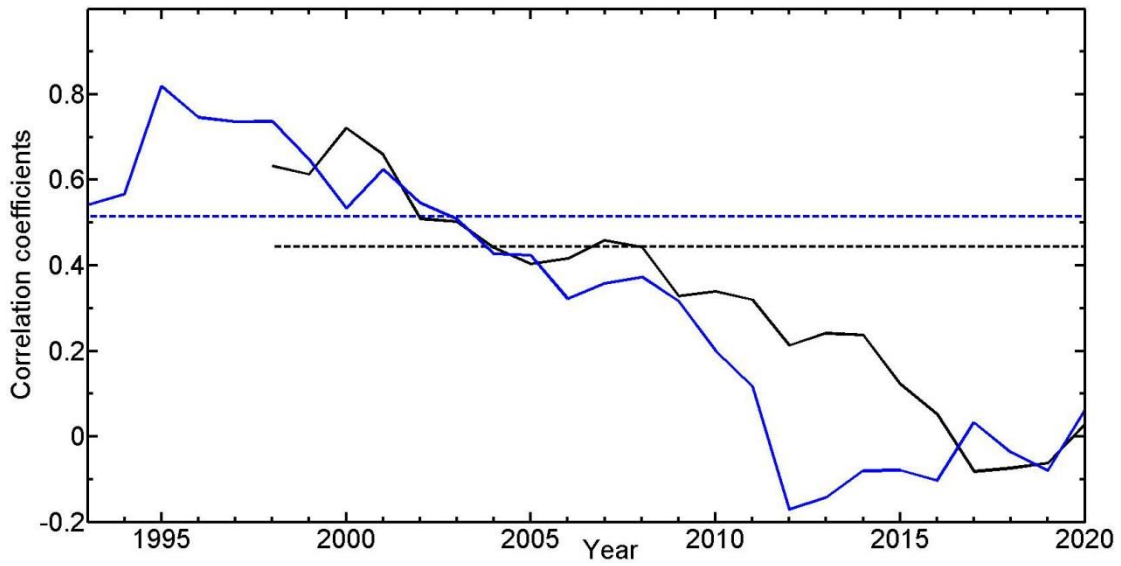
393

394 Figure 2 Moving correlations of the detrended and ENSO-signal-removed SIOD and SAOD
395 indices using a 20-year (black solid line) and a 15-year (blue solid line) sliding window.   Dashed
396 lines denote the correlation coefficients with the 95% confidence level for 20 (black) and 15 (blue)
397 samples. Abscissa indicates the end year of the moving correlations. The above results are
398 obtained using the Kaplan Extended SST V2 data.

399
400
401
402
403
404
405
406
407
408
409
410
411
412
413
414
415
416
417
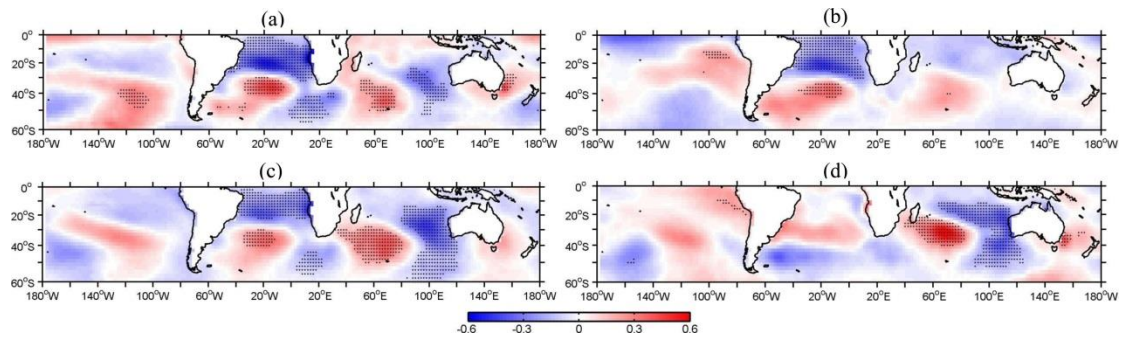
418

419 Figure 3. Regression maps of the SST anomalies (℃) onto the summertime indices of (a), (b)

420 SAOD and (c), (d) SIOD, over the periods of (a), (c) 1979-1999 and (b), (d) 2000-2020. Dots

421 denote the regions of above 95% confidence level.

422

423

424

425

426

427

428

429

430

431

432

433

434

435

436

437

438

439

440

441

442

443

444

445

446

447

448

449

450

451

452

453

454
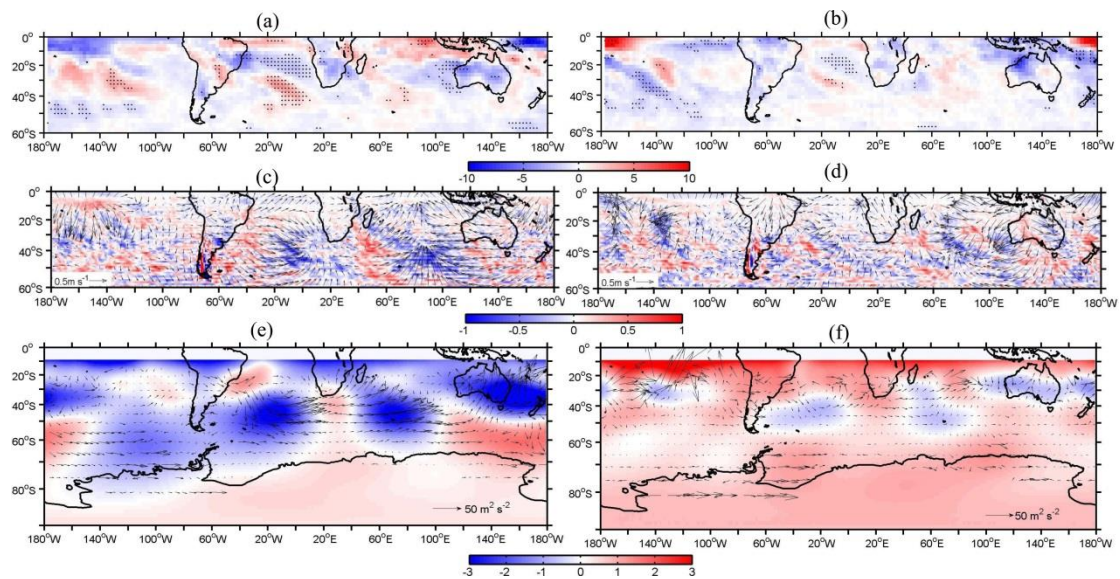
Figure 4. Regression maps of (a), (b) the anomalous outgoing longwave radiation (OLR) (W m^{-2}) at the top of the atmosphere, (c), (d) Rossby wave source (RWS) (10^{-10}s^{-2}) and 200-hPa divergent wind (vector), and (e), (f) wave activity flux (WAF) (vector) and streamfunction (m^2 s^{-1}) onto the summertime SAOD index over the periods of (a), (c), (e) 1979-1999 and (b), (d), (f) 2000-2020.
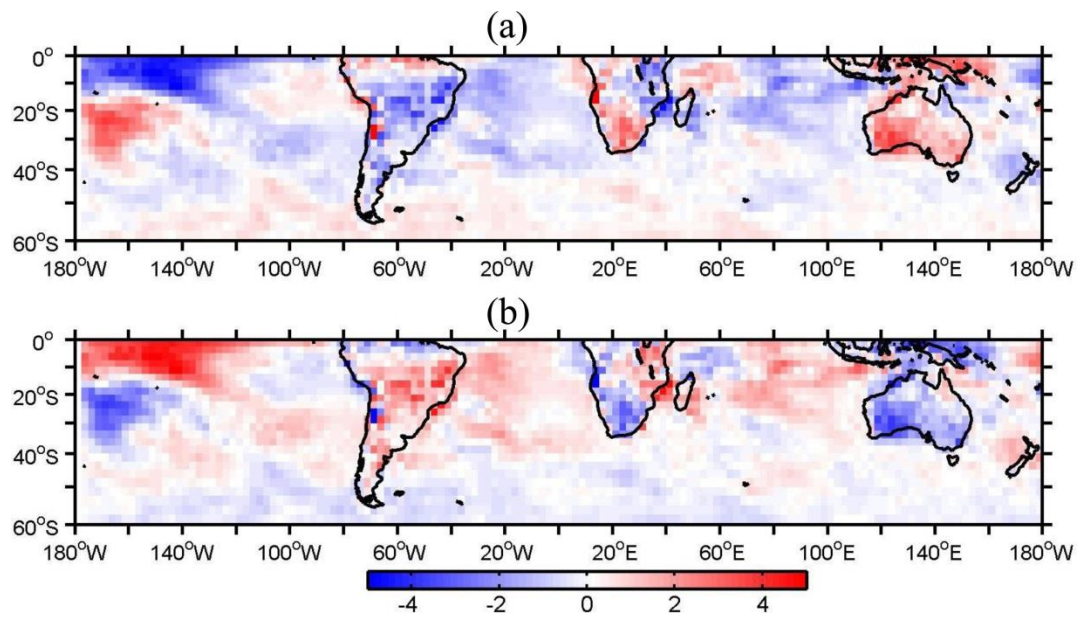
Figure 5. Climatological OLR anomalies (W m^{-2}) during (a) 1979-1999 and (b) 2000-2020, with respect to the 42-year climatology over the 1979-2020 period.

486
487
488
489
490
491
492
493
494
495
496
497
498
499
500
501
502
503
504
505
506
507
508
509
510
511
512
513
514
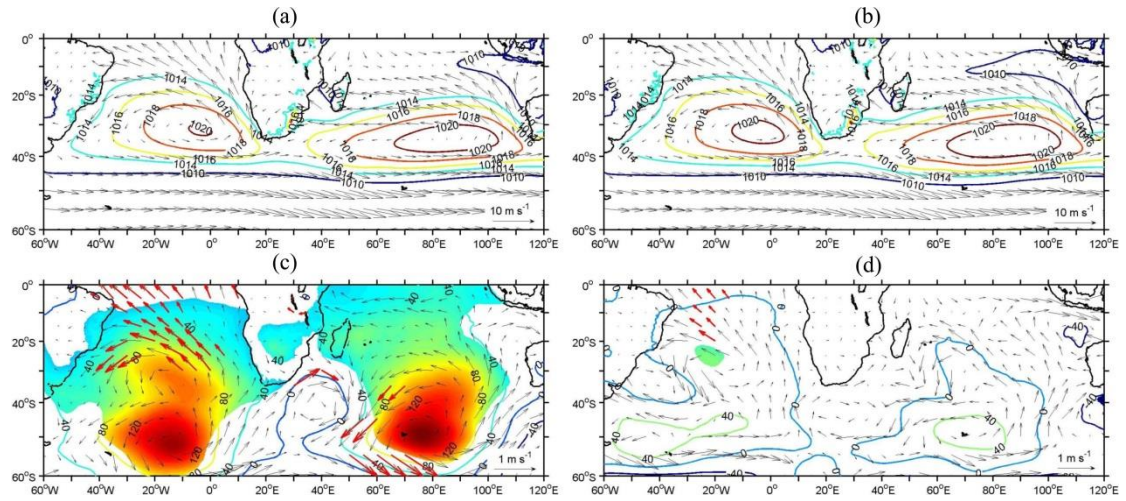
Figure 6. Climatological mean sea level pressure (MSLP, in hPa) and 10-m wind field (vector) over the periods of (a) 1979-1999 and (b) 2000-2020, and regression maps of MSLP (in Pa) and 10-m wind field (vector) onto the summertime SAOD index over the periods of (c) 1979-1999 and (d) 2000-2020. Shaded regions and red vectors indicate above 95% confidence level.
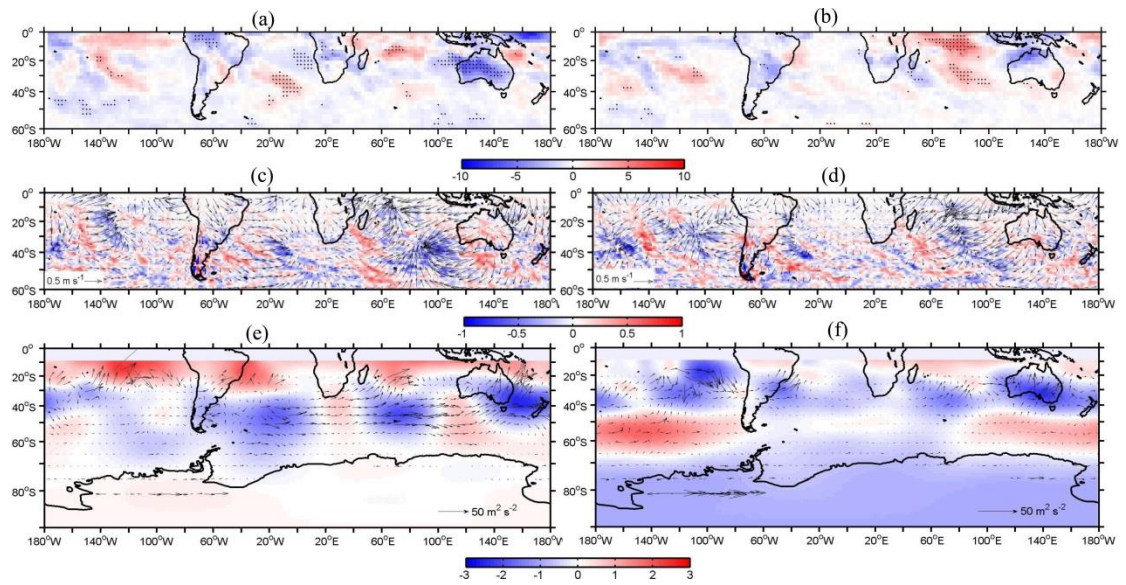
Figure 7. Regression maps of (a), (b) OLR (W m^{-2}), (c), (d) RWS (10^{-10} s^{-2}) and 200-hPa divergent wind (vector), (e), (f) WAF (vector) and streamfunction (m^2 s^{-1}) onto the summertime SIOD index over the 1979-1999 period (a), (c), (e) and the 2000-2020 period (b), (d), (f).
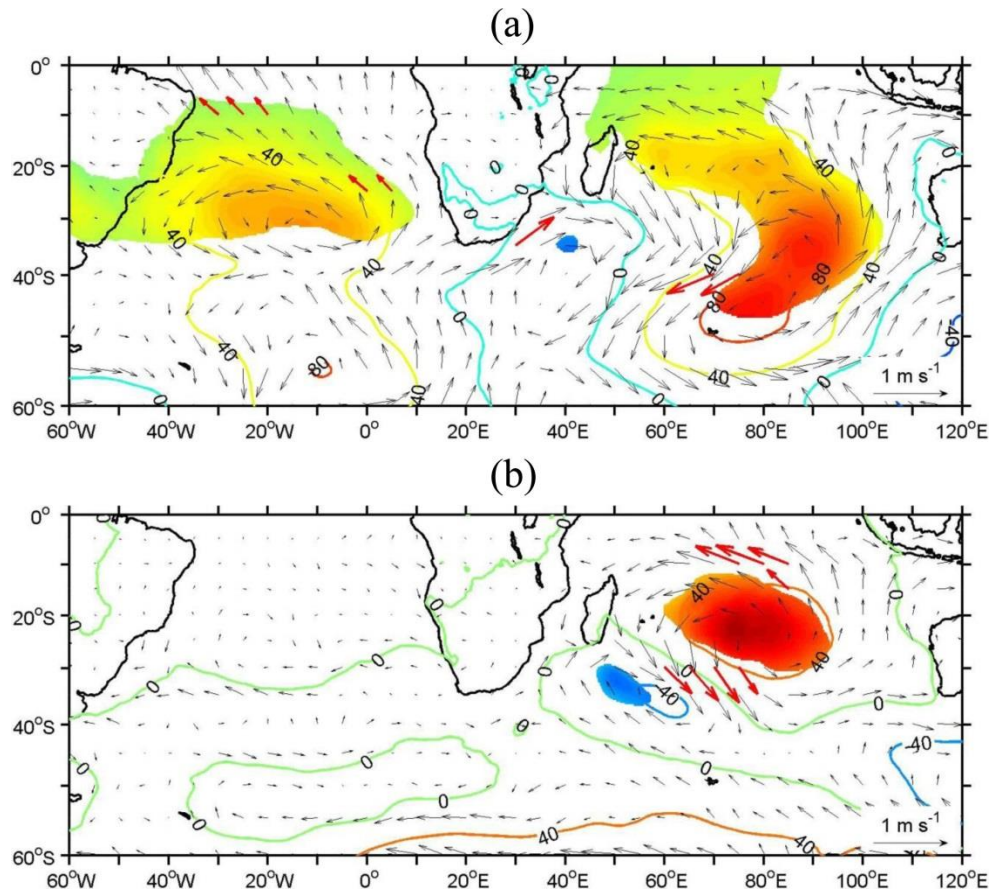
Figure 8. Regression maps of MSLP (in Pa) and 10-m wind field (vector) onto the summertime
SIOD index over the periods of (a) 1979-1999 and (b) 2000-2020. Shaded regions and red vectors
indicate above 95% confidence level.